Novel Composite Hydrogen-Permeable Membranes for Non-Thermal Plasma Reactors for the Decomposition of Hydrogen Sulfide

Quarterly
April 1, 2004
June 30, 2004

Morris D. Argyle
John F. Ackerman
Suresh Muknahallipatna
Jerry C. Hamann
Stanislaw Legowski
Ji-Jun Zhang
Guibing Zhao
Robyn J. Alcanzare
Linna Wang
Ovid A. Plumb

July 2004

DE-FC26-03NT41963

University of Wyoming
Department of Chemical and Petroleum Engineering
Department of Electrical and Computer Engineering
Dept. 3295
1000 East University Avenue
Laramie, WY 82071

Disclaimer

Abstract

The goal of this experimental project is to design and fabricate a reactor and membrane test cell to dissociate hydrogen sulfide (H_2S) in a non-thermal plasma and recover hydrogen (H_2) through a superpermeable multi-layer membrane. Superpermeability of hydrogen atoms (H) has been reported by some researchers using membranes made of Group V transition metals (niobium, tantalum, vanadium, and their alloys), although it has yet to be confirmed in this study. Experiments involving methane conversion reactions were conducted with a preliminary pulsed corona discharge reactor design in order to test and improve the reactor and membrane designs using a non-toxic reactant.

This report details the direct methane conversion experiments to produce hydrogen, acetylene, and higher hydrocarbons utilizing a co-axial cylinder (CAC) corona discharge reactor, pulsed with a thyratron switch. The reactor was designed to accommodate relatively high flow rates (655×10^{-6} m^3/s) representing a pilot scale easily converted to commercial scale. Parameters expected to influence methane conversion including pulse frequency, charge voltage, capacitance, residence time, and electrode material were investigated. Conversion, selectivity and energy consumption were measured or estimated. C_2 and C_3 hydrocarbon products were analyzed with a residual gas analyzer (RGA). In order to obtain quantitative results, the complex sample spectra were de-convoluted via a linear least squares method. Methane conversion as high as 51% was achieved. The products are typically 50% - 60% acetylene, 20% propane, 10% ethane and ethylene, and 5% propylene. First Law thermodynamic energy efficiencies for the system (electrical and reactor) were estimated to range from 38% to 6%, with the highest efficiencies occurring at short residence time and low power input (low specific energy) where conversion is the lowest (less than 5%). The highest methane conversion of 51% occurred at a residence time of 18.8 s with a flow rate of $39.4 \times 10^{-6} m^3$/s (5 ft^3/h) and a specific energy of 13,000 J/l using niobium and platinum coated stainless steel tubes as cathodes. Under these conditions, the First Law efficiency for the system was 8%. Under similar reaction conditions, methane conversions were ~50% higher with niobium and platinum coated stainless steel cathodes than with a stainless steel cathode.

Table of Contents

List of Graphical Materials

Introduction

Hydrogen sulfide (H_2S) is a naturally occurring gas found in some natural gas deposits, but it is also produced industrially during chemical processes, particularly in the petroleum refining industry during sulfur removal from crude oils.[1,2] Currently, most of this H_2S is converted into water and elemental sulfur through a series of combustion and reduction reactions known as the Claus process.[2,3] The Claus process is not completely efficient, which results in some SO_2 and H_2S emissions to the environment or the process requires additional costly treatment steps (known as tail gas clean-up) in order to limit sulfur emissions to acceptable levels. Further, the Claus process wastes a potential hydrogen resource by converting the hydrogen (H_2) contained in H_2S into thermodynamically stable water.[2,3]

Previous studies using thermal or catalytic decomposition of H_2S to recover H_2 and elemental sulfur have demonstrated that this conversion is feasible, but the results have not been economically viable due to large energy requirements associated with high reaction temperatures.[4-8] Typical required reaction temperatures are 800°C for the catalytic systems and 2000°C for complete thermal decomposition.[5] Other researchers have used plasma reactors to dissociate H_2S, but again the energy efficiency of the processes has been low, presumably because many successive dissociation-recombination processes serve only to recreate the reactant H_2S and produce heat before H_2 is finally formed as a product.[9-16] Most of these researchers have reported energy requirements of 0.5 to 200 eV/molecule of H_2S converted,[12,16] which is many times higher than the theoretical minimum of ~0.2 eV/molecule H_2S (21 kJ/mol H_2S) based on the enthalpy of formation of H_2S at 298 K.[17] The intent of this project is to efficiently recover the product H_2 from H_2S decomposition by using a membrane to drive the reaction to completion. The membrane removes the hydrogen by transporting the H atoms out of the reaction chamber as they are formed. Thus, the electrical power requirements for decomposing the H_2S should approach the theoretical minimum.

Before beginning the H_2S experiments, methane decomposition experiments were performed to prove the reactor design using a non-toxic gas. Methane decomposes in the plasma to form H_2 and higher hydrocarbons and thus provides a surrogate reactant to test hydrogen permeation rates through the test membranes.

The conversion of natural gas (typically 75% by weight methane) to hydrogen and more valuable higher molecular weight hydrocarbons, such as acetylene, is of great importance to the petrochemical industry. Direct conversion of methane using various plasma processing technologies has been studied for many years with significantly more attention since the 1980's.[18-37] Several types of discharges, including AC and DC corona discharges, dielectric-barrier discharge, arc plasma and the combination of microwave plasma and catalysts have been reported to produce acetylene, ethylene, hydrogen, methanol, and other liquid products.[18-22] The direct conversion of methane into acetylene in a thermal arc plasma, developed by Hüls,[20] has been used for more than 40 years by Dupont.[21] This process has also been used for hydrogen production.[22] However, thermal plasmas are a highly energetic state of matter characterized by extremely high temperatures[20, 23-26] and a high degree of ionization resulting in the need for specialized materials of construction. High temperature plasma processes typically exhibit low energy efficiency.

Since the 1980s, applications of non-thermal plasmas have been investigated as a promising alternate, low temperature method to convert methane to higher hydrocarbons. Non-thermal plasmas can be produced either by electron beam irradiation or electrical discharge, where the majority of the energy input goes into the production of energetic electrons rather than heating of the gas. Non-thermal plasmas have advantages over other processes in realizing thermodynamically unfavorable reactions due to potential non-equilibrium conditions.[27] These processes also overcome the disadvantage of the high temperature required by conventional catalytic processes. Effective plasma chemical reactions occur in the streamer-type negative and positive pulse corona discharge regime. The electrons in the corona primary streamer head possess an average energy in the range of 10-20 eV, which is sufficient for ionization of methane molecules and decomposition to CH_2 radicals.[22] The gas molecules in a plasma reactor are near room temperature, while the electron temperature is higher than 10^4 K. At such high temperatures, the energy of an electron is greater than 50 kcal·mol^{-1}. This results in conventional reactions which normally proceed at an appreciable rate only at a very high temperature being completed at a lower temperature in a radio frequency (RF) non-thermal plasma reactor[27] and similarly in other non-thermal plasma reactors.

Yao *et al.*[18,19] reported that a non-thermal pulsed plasma with a high pulse frequency can be used to convert methane to acetylene, with high acetylene selectivity and high methane conversion at room temperature and atmospheric pressure. In their results, pulse frequency is the most important factor influencing acetylene selectivity and methane conversion rate. Results indicate that the high-frequency pulsed plasma is competitive with commercial acetylene production processes. Also, the temperature of the background methane gas does not markedly influence methane conversion in the temperature range from 20˚C to 200˚C. At a flow rate of 150 ml/min, the methane conversion was 40% at 6 kHz[18] pulse frequency. In addition, Yao *et al.*[28] utilized a high-frequency pulsed plasma (HFPP) point-to-point reactor to convert CH_4 to C_2H_2 and H_2. Compared with conventional arc and partial oxidation processes, Yao *et al.*[28] concluded that the HFPP process would have the lowest operating and capital cost with energy efficiency higher than 72%. At a flow rate of 300 ml/min (0.64 ft^3/h), they reported 39% conversion. Yang[22,29] used dielectric barrier discharges (DBD) and corona discharges (CD) to convert methane. For the DBD, the primary products were ethane and propane. In the AC corona discharge reactor with flow rate of 20 ml/min (0.042 ft^3/h), the conversion was 67%. From these studies, the primary product yields for each reactor are a unique function of the specific energy input and independent of the reactor size and whether the gas flow or the power input is varied or fixed. Hsieh *et al.*[27] obtained CH_4 conversion of 80%, with flow rate of 50 ml/min (0.11 ft^3/h) using a radio frequency plasma reactor. They concluded that decreasing the mean free paths of the reactants at higher operational pressures resulted in less acceleration of ions and electrons and hence fewer reactions. Zhu *et al.*[30] obtained 44.6% methane conversion at an input energy density of 1788 kJ/mol and a pulse repetition frequency of 66 Hz. Their experiments were completed in a co-axial cylinder (CAC) non-thermal plasma reactor with flow rate of 1.12 mmol/min. Zhang *et al.*[31] studied direct methane conversion to C_2 hydrocarbons at elevated pressure using a pulsed microwave plasma. With a flow rate of 300 ml/min (0.64 ft^3/h) and 120 W of power, methane conversion reached 59.2%.

To summarize, the flow rate for previous investigations[18-22, 27-41] has been limited to less than 300 ml/min (0.64 ft^3/h), which is far from practical for a commercial operation. The primary shortcomings of non-thermal plasma technology for methane

conversion are higher energy consumption or low energy efficiency and low selectivity towards desired hydrocarbons.[22] The design and characterization of larger reactors that can accommodate high throughput are critical if these types of reactors are to be applied successfully in commercial operations.

In this study, a co-axial cylinder pulsed corona reactor driven by a thyratron switch is used to investigate the direct conversion of methane a flow rates up to 655×10^{-6} m^3/s (80 ft^3/h). The grid of the thyratron, which acts as a control element, initiates the conduction or breakdown to generate branched streamer coronas by discharging the energy stored in a bank of capacitors to the electrode. Parameters expected to influence methane conversion are investigated, including pulse frequency, charge voltage, capacitance, residence time, and cathode composition.

Executive Summary

Hydrogen sulfide (H$_2$S) is a potential resource for the production of molecular hydrogen (H$_2$) that is currently being lost because the established industrial Claus process converts H$_2$S into water and elemental sulfur. This project seeks to recover H$_2$ from H$_2$S by combining plasma reactor processing with multi-layer membranes to efficiently dissociate H$_2$S and recover the H$_2$ in a pure form. Experiments with a preliminary design of a pulsed corona discharge reactor have been conducted initially on methane conversion reaction due to safety considerations.

The project has six main tasks: staffing, procurement of equipment and supplies, membrane fabrication, permeation cell fabrication, membrane evaluation, and reports and briefings. Staffing the project has been completed, although with some set-backs during the process. Procurement of equipment and supplies, membrane fabrication, membrane evaluation, and the reporting tasks are all on-going. An experimental reactor and permeation cell has been fabricated and used extensively for methane decomposition experiments, the details of which are included in this report. Based on experience with this test cell, an improved reactor will be constructed that will incorporate additional ideas that are generated from the initial H$_2$S experiments. A niobium membrane has been evaluated for hydrogen permeability during the methane experiments, but it does not appear that superpermeability has been achieved. Further experiments are underway to verify this result. The project is slightly behind schedule with regard to H$_2$S decomposition experiments, which were scheduled to begin during this reporting quarter. Unanticipated requirements imposed by the University of Wyoming's Safety Office forced a delay in the H$_2$S experiments, but the methane experiments conducted in the interim have provided extensive experience in both experimental technique and equipment design. This experience and knowledge are expected to allow the project to return to schedule when the H$_2$S experiments begin.

This report includes results of direct methane conversion experiments to produce hydrogen, acetylene, and higher hydrocarbons utilizing a co-axial cylinder corona discharge reactor, pulsed with a thyratron switch. Parameters expected to influence methane conversion including pulse frequency, charge voltage, capacitance, residence time, and electrode material were investigated. Power input appears to be the most important parameter, but the other parameters appear to have some smaller independent effects. Conversion, selectivity and energy consumption were measured or estimated. The products were measured and analyzed by standard mass spectroscopic techniques. Methane conversion as high as 51% was achieved. The products were typically 50% - 60% acetylene, 20% propane, 10% ethane and ethylene, and 5% propylene. Thermodynamic energy efficiencies for the system are estimated to range from 38% to 6%, with the highest efficiencies occurring at short residence time and low power input (low specific energy) where conversion is the lowest (less than 5%). The effect of cathode material was probed using stainless steel, platinum coated stainless steel, and niobium membrane tubes. Under similar reaction conditions, methane conversions were ~50% higher with the niobium membrane and platinum coated stainless steel cathodes than with a stainless steel cathode. The highest methane conversion of 51% occurred at a

residence time of 18.8 s with a methane flow rate of $39.4 \times 10^{-6} m^3/s$ (5 ft^3/h) and a specific energy of 13,000 J/l using niobium and platinum coated stainless steel tubes as cathodes. Under these conditions, the energy efficiency for the system was 8%.

This study involves the same experimental techniques and equipment that will be used during the initial H_2S decomposition experiments. An understanding of the reaction parameter space, which includes pulse frequency, discharge capacitance and voltage, reactor residence time, and electrode material, is vital to optimize reactor performance and energy efficiency. The effect of electrode material on the corona discharge and reaction efficiency is particularly important because the multi-layered membranes which will be used as electrodes during H_2S decomposition may alter the corona discharge in an unpredictable manner. Although the electrode effect may not be predictable at this point, knowledge of its existence, as well as the other parameters, will streamline the H_2S experiments.

The data presented in this report were obtained using an older reactor design that has been modified as a result of the methane conversion experiments. The reactor energy efficiency appears to have improved by 30 to 50% compared to the old design. While these improved energy efficiency results are still too low for commercial application, they emphasize the need for efficient membranes to remove hydrogen and drive the reaction toward completion. The insight gained from these methane experiments will be incorporated into the H_2S decomposition experimental and equipment designs. (The data from the new reactor design were not complete at the end of the quarter and have not been included in this report. However, these new results will be included in a paper being prepared for submission in a peer-reviewed journal.)

Experimental

      Experimental apparatus: Figure 1 shows the system layout. It consists of the electrical system built around a thyratron switch, a flow control and distribution system, and a gas sampling system. The reactor is oriented vertically with the gas flow from bottom to top. The electrical system can deliver charge voltage from 10 kV to 25 kV and pulse frequencies from 0 to 1000 Hz. The capacitor bank provides space for four "doorknob" capacitors, in increments of 640 pF. The thyratron switch element is cooled with compressed air. The capacitors are charged to the desired voltage using a 40 kV oil cooled high voltage power supply. On triggering the thyratron, the stored energy in the capacitors is discharged in a few nanoseconds to the anode, giving rise to a high rate of change of voltage (dV/dt) on the anode. This high voltage applied to the reactor anode causes the breakdown of gases flowing through the reactor, creating plasma. The process of charging and discharging of the capacitors is repeated based on the thyratron trigger frequency and leads to sustained current streamers or plasma. The electrical control unit is connected to the reactor through an outer 0.9144 m (3 ft) long by 0.0462 m (1.8") inside diameter (ID) stainless steel tube with 4.6 mm (0.18") wall thickness that provides structural support and a shell around the electrodes. Experiments were conducted using three different interior tubes that serve as the cathode. These were also 0.9144 m (3 ft) long and included a 0.0244 m (0.96") ID, 0.5 mm (0.02") wall thickness stainless steel tube, a 0.0238 m (0.94") ID, 0.76 mm (0.03") wall thickness niobium membrane, and a stainless steel tube coated with a 100 nm (4×10^{-6} in) thick layer of platinum. A stainless steel wire running through the center of the interior tube served as the anode. The outside diameter (OD) of the wire was 0.71 mm (0.028") for experiments with 2 capacitors and 1.143 mm (0.045") for 4 capacitor experiments. The experiments were carried out with the inlet gas at room temperature and 198 kPa absolute pressure (14 psig). Experiments were initiated by purging the entire piping system with pure CH_4 (Air Gas Company, ultra high purity) three times. Pure methane was introduced from a gas cylinder and the flow rate was measured by a rotameter (±2% accuracy). Steady state operating conditions (pressure and flow rate) were typically achieved after three minutes. This was determined by sampling the exhaust gases with a Residual Gas Analyzer (RGA, Stanford Research Systems, Inc. QMS100).
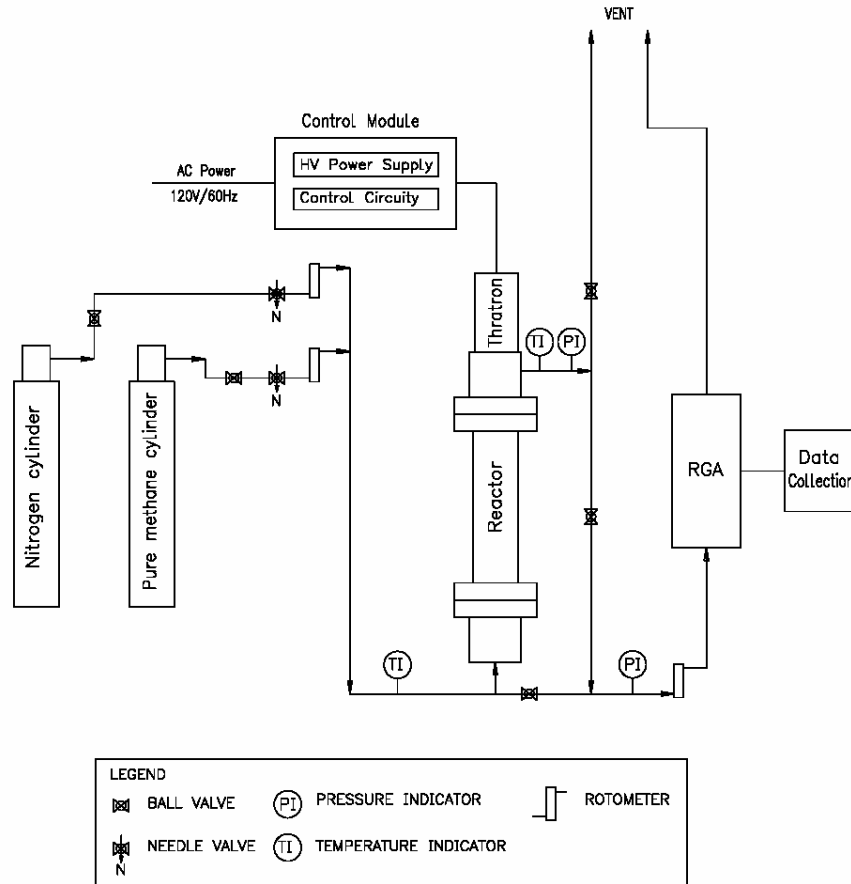
Figure 1. Experimental setup

Measurements of concentration were carried out with the RGA, which is a simplified mass spectrometer with quadrupole probe.[42] To perform quantitative measurements, the instrument was calibrated for H_2, CH_4, C_2H_2, C_2H_4, C_2H_6, C_3H_6 and C_3H_8 using gases of certified composition. The sensitivity for each of the components is shown in Table 1. The hydrocarbon samples in the source chamber are ionized to create fragments of different masses. Each specific hydrocarbon has its own characteristic peak. The intensity of each selected ion in the mass spectrum can be described mathematically as follows:[43]

$$I(m) = \sum_j S(m, j) \cdot P(j) \tag{1}$$

where $I(m)$ is the measured current intensity at mass m, $S(m, j)$ is the sensitivity factor of component j at mass m, and $P(j)$ is the partial pressure for component j. The number of selected current intensities must be greater than the number of components to obtain quantitative results.

The sample spectra are de-convoluted using the linear least squares method, which can be expressed as:

$$\vec{P} = (S^t \cdot S)^{-1} \cdot S^t \cdot \vec{I} \tag{2}$$

where $\vec{P}$ is the vector of estimated partial pressure for every component, $\vec{I}$ is the vector containing the measured current intensities, S is the two dimensional matrix containing the sensitivity factor of each component at specified mass m, and S^t is the transpose of S.

Table 1. Sensitivity factors for RGA ($\times 10^{-4}$ A/Torr)

Selected mass	Component						
	Hydrogen H_2	Methane CH_4	Acetylene C_2H_2	Ethylene C_2H_4	Ethane C_2H_6	Propylene C_3H_6	Propane C_3H_8
2	15.747						
13			0.0844				
14		0.1410					
15		1.3169					0.0370
16		1.6791					
24			0.0905				
25			0.3579	0.1057			
26			2.0220	0.7224	0.3349	0.0786	0.0719
27				0.7994	0.4458	0.3328	0.3782
28				1.5379	1.6479		0.9879
29					0.2922		1.2073
30					0.4509		
39						0.7556	0.1619
40						0.2889	
41						1.3695	0.1570
42						0.9917	
43							0.3731
44							0.4536

Definitions: Methane conversion is defined as:

$$X\% = 100\% \times \frac{N_0 - N}{N_0} = 100\% \times \frac{F_0 \times x_0 - F_1 \times x_1}{F_0 \times x_0} \tag{3}$$

where $X\%$ is CH_4 conversion, N_0, F_0, x_0 represent moles, flow rate and mole fraction of methane at the inlet, respectively, and N, F_1, x_1 represent moles, flow rate, and mole fraction of methane at the outlet, respectively.

Selectivity is calculated as

$$S_{Cn}\% = \frac{F_1 \times x_{Cn} \times n}{F_0 \times x_0 - F_1 \times x_1} \times 100\% \tag{4}$$

where S_{Cn} represents the selectivity to C_2 or C_3 hydrocarbons or H_2, n is the molecular carbon number of the hydrocarbons or 0.5 for H_2, and x_{Cn} is the mole fraction of C_2 or C_3 hydrocarbons or H_2 at the outlet. The power input to the reactor is estimated as

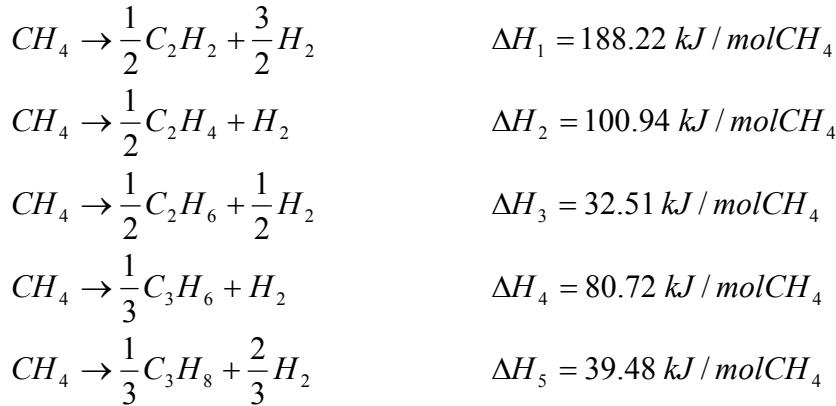$$W = 0.5 \times (C \times V^2) \times f \tag{5}$$

where W is the input power in watts, C is the capacitance in farads, V is the charge voltage in volts and f is the pulse frequency in Hz. Equation (5) is an estimate of the total power input to the system and includes electrical losses. The specific energy (J/l) for the conversion of methane is defined as

$$W_p = W / F_0 \tag{6}$$

The system energy efficiency, η, based on the First Law can then be calculated

$$\eta = \frac{\sum_i \Delta H_i \times Y_{Cn} \times n}{W} \times 100\% \tag{7}$$

where H_i is the enthalpy of reaction for the i-th reaction for C_2 and C_3 hydrocarbon production. The specific reactions considered are as follows:

$$CH_4 \to \frac{1}{2} C_2 H_2 + \frac{3}{2} H_2 \qquad\qquad \Delta H_1 = 188.22\ kJ / molCH_4$$

$$CH_4 \to \frac{1}{2} C_2 H_4 + H_2 \qquad\qquad \Delta H_2 = 100.94\ kJ / molCH_4$$

$$CH_4 \to \frac{1}{2} C_2 H_6 + \frac{1}{2} H_2 \qquad\qquad \Delta H_3 = 32.51\ kJ / molCH_4$$

$$CH_4 \to \frac{1}{3} C_3 H_6 + H_2 \qquad\qquad \Delta H_4 = 80.72\ kJ / molCH_4$$

$$CH_4 \to \frac{1}{3} C_3 H_8 + \frac{2}{3} H_2 \qquad\qquad \Delta H_5 = 39.48\ kJ / molCH_4$$

The yield, Y_{cn} of C_2 and C_3 hydrocarbons is calculated from equation (8)

$$Y_{Cn} = X\% \times S_{Cn}\% / 100 = \frac{F_1 \times x_1}{F_0 \times x_0} \times 100\% \tag{8}$$

Results and Discussion

Experimental conditions are shown in Table 2. Experiments were carried out at 300, 450, 600, 800 and 1000 Hz pulse frequency at flow rates ranging from 39.4-630 $\times 10^{-6}$ m^3/s (5 to 80

10

ft^3/h) resulting in residence times from 18.8 to 1.18 s. Charge voltage ranged from 15 to 25 kV, although the majority of the results were acquired using a charge voltage of 20 kV. Capacitance was fixed at either 1280 or 2560 pF. Figures 2, 3 and 4 show the effect of the three electrical parameters, frequency, capacitance and voltage, on methane conversion. Figure 5 shows conversion as a function of specific energy, while Figure 6 illustrates the effect of residence time. Figure 7 and 8 illustrate the influence of electrode material on methane conversion. Figure 9 depicts the composition of the products. Figure 10 shows the variation of the hydrogen to carbon ratio in the products, including hydrogen. Each figure will be discussed in detail.

Table 2. Experiment conditions

Tube	Flowrate ($\times 10^{-6}$ m^3/s)	Residence time (s)	Charge voltage (kV)	Frequency (Hz)	Pressure (psig)	Capacitance (pF)
SS	39.4	18.8	20, 23	300, 450, 600, 800, 1000	14	1280, 2560
	78.7	9.38	15, 20, 25	300, 450, 600, 800, 1000	14	1280
	157	4.69	15, 20, 25	300, 450, 600, 800, 1000	14	1280
	315	2.35	20, 23	300, 450, 600, 800, 1000	14	1280
	630	1.18	20, 23	300, 450, 600, 800, 1000	14	1280
Nb	39.4	18.8	20	300,450,600,800,1000	14	2560
Pt/SS	39.4	18.8	20	300,450,600,800,1000	14	2560

Influence of pulse frequency on methane conversion: Figure 2 illustrates the influence of pulse frequency on methane conversion. Conversion increases with frequency at all residence times. This trend of increasing conversion likely continues for frequencies higher than 1000 Hz. The time delay between pulses at 1000 Hz seems to be more than sufficient to allow completion of the reactions before initiating the next series of reactions with another pulse.[18] The power input is directly related to frequency. Thus, the horizontal axis for Figure 2 can be changed to power by simply changing scales. The results in Figure 2 suggest that specific energy is the primary factor influencing methane conversion. This is illustrated in Figure 5 and will be discussed later. The methane temperature is reported[18] to reach ~2500 K in the discharge streamer, which suggests that methane conversion in the streamer discharge is similar to pyrolysis. The concentrations of ionic species are very small and therefore the reactions of ionic species may be ignored.[44] The recognized CH$_4$ dissociation reactions are as follows:[18, 28, 33]:

$$CH_4 + e \rightarrow CH_3 + H + e \qquad\qquad\qquad\qquad\qquad\qquad\qquad\text{(R1)}$$

$$CH_4 + e \rightarrow CH_2 + 2H + e \qquad\qquad\qquad\qquad\qquad\qquad\quad\text{(R2)}$$

$$CH_4 + e \rightarrow CH + 3H + e \qquad\qquad\qquad\qquad\qquad\qquad\quad\text{(R3)}$$

$$CH_4 + e \rightarrow C + 4H + e \qquad\qquad\qquad\qquad\qquad\qquad\qquad\text{(R4)}$$

$$CH_3 + e \rightarrow CH_2 + H + e \qquad\qquad\qquad\qquad\qquad\qquad\quad\text{(R5)}$$

$$CH_2 + e \rightarrow CH + H + e \qquad\qquad\qquad\qquad\qquad\qquad\qquad\text{(R6)}$$

$$CH + e \rightarrow C + H + e \qquad\qquad\qquad\qquad\qquad\qquad\qquad\quad\text{(R7)}$$

Higher pulse frequency means shorter delay time between pulses. The reactions are more effective if the active reactants (radicals or ions) produced in the previous pulse streamer are still available to promote the next pulse discharge.[19] In addition, more energy is discharged in to the reactor at higher pulse frequencies, indicating more radicals can be produced to drive reactions (R1)-(R7).
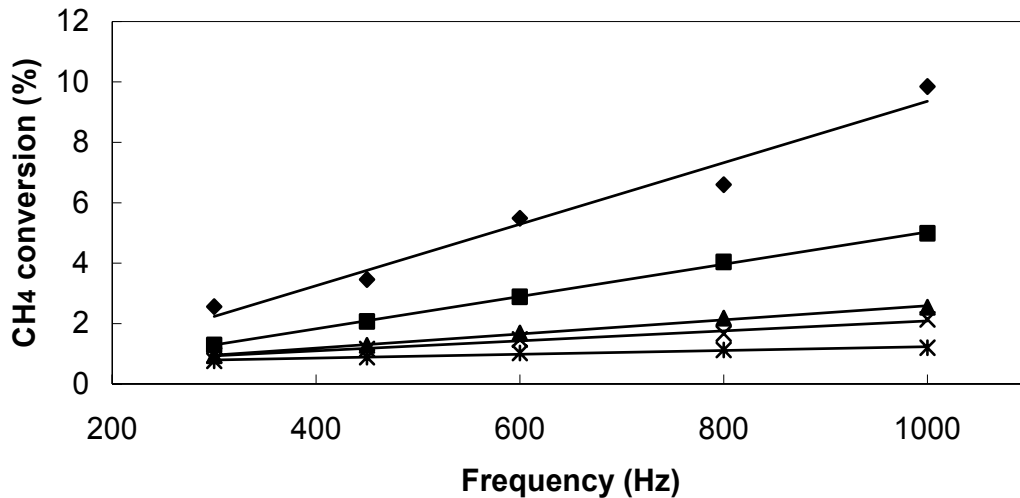
Operating parameters: 20kV, 1280pF, 14psig, pure CH_4, SS tube

	Flowrate / residence time ($\times10^{-6}m^3/s$ / s)		Flowrate / residence time ($\times10^{-6}m^3/s$ / s)
◆—	39.35 / 18.76	■—	78.7 / 9.38
▲—	157.4 / 4.69	×—	314.8 / 2.35
*—	629.6 / 1.175		

Figure 2. Methane conversion as a function of pulse frequency and methane flow rate.

Influence of charge capacitance on methane conversion: Figure 3 illustrates that charge capacitance has a significant effect on conversion. The highest methane conversion with the stainless steel cathode (33.8%) occurred at the highest specific energy input (with 2560 pF, residence time of 18.8 s, 1000 Hz and a charge voltage of 20 kV). This is over than 3 times the conversion (9.85%) achieved at half of the power input (with 1280 pF and the same frequency, residence time, and charge voltage). This implies that the energy delivered per pulse is the critical parameter effecting conversion.
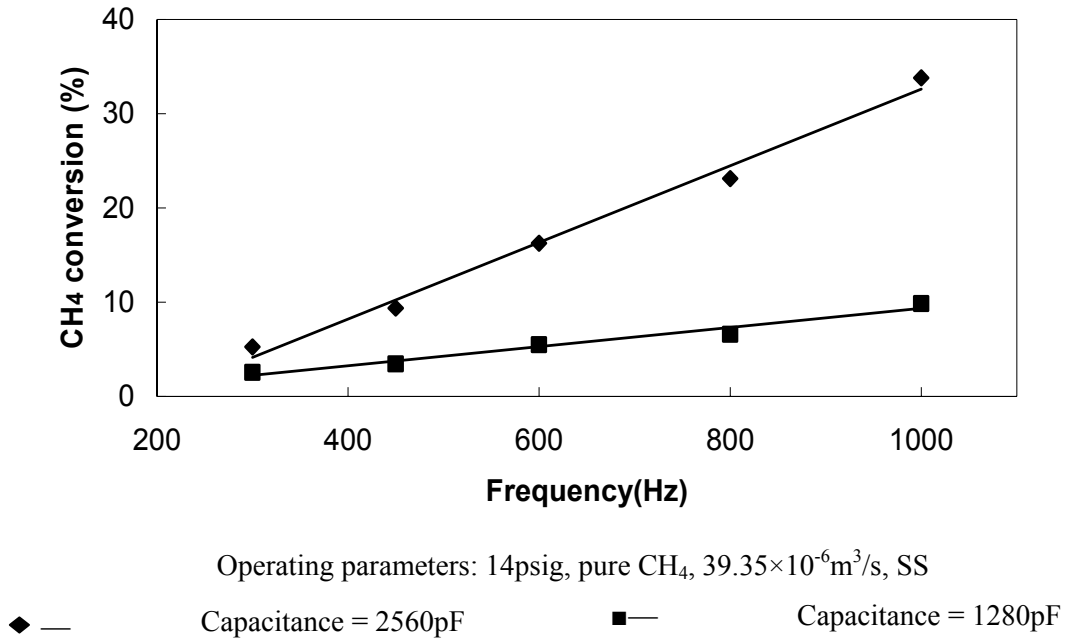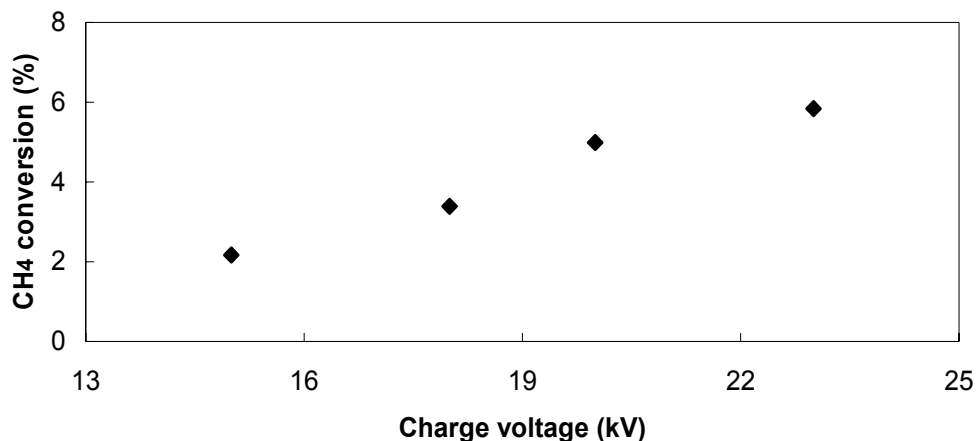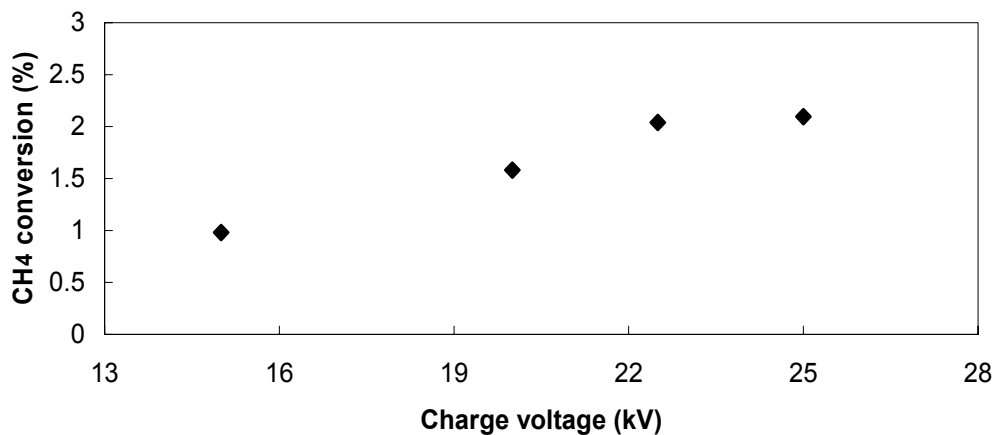

Operating parameters: 14psig, pure CH_4, $39.35 \times 10^{-6} m^3/s$, SS

◆ —   Capacitance = 2560pF   ■ —   Capacitance = 1280pF

Figure 3. The effect of charge capacitance on methane conversion.

Influence of charge voltage on methane conversion: Figure 4 shows the effect of charge voltage on methane conversion. Two experiments were conducted to examine the effect of charge voltage using the stainless steel tube as the cathode. One was performed at a residence time of 9.38 s with a methane flow rate of 78.7×10^{-6} m^3/s (10 ft^3/h) and 1000 Hz, while the other had a residence time of 4.69 s, 157×10^{-6} m^3/s (20 ft^3/h), and 600 Hz. The range of possible charge voltages is limited to that range which produces a corona discharge, given the reactor geometry, gas pressure, and gas composition. This range is roughly 15 to 25 kV for our reactor and operating conditions. Methane conversion increases with the increase of charge voltage for all flow rates. Within this voltage range, the conversion is expected to increase parabolically

because of the relationship between power or specific energy and voltage (Eq. 5). At the three lower charge voltages, the relationship between methane conversion and charge voltage appears to be parabolic, but this trend does not continue at highest charge voltage. This phenomenon may be explained by Paschen's law,[45] which describes the functional relationship between charge voltage, gas pressure, and geometry for the formation of a stable discharge. The data suggest that ~25 kV may be the limit at which the discharge changes from corona to arcing, resulting in a decrease in reactor performance.

Operating parameters: 1280pF, 14psig, pure CH_4, 78.7×10^{-6}m^3/s, 1000Hz, SS tube

Operating parameters: 1280pF, 14psig, pure CH_4, 157.4×10^{-6}m^3/s, 600Hz, SS tube

Figure 4. Methane conversion as a function of charge voltage.

Influence of specific energy on methane conversion: Figure 5 illustrates the relationship between the specific energy and methane conversion in the stainless steel cathode

for data covering a range of frequency, capacitance and residence time at fixed voltage. Methane conversion increases somewhat monotonically with increasing specific energy. This suggests that capacitance has an effect on conversion beyond that resulting from changing specific energy, whereas frequency and residence time only effect specific energy. From the standpoint of system design, specific energy appears to by the key factor influencing methane conversion.
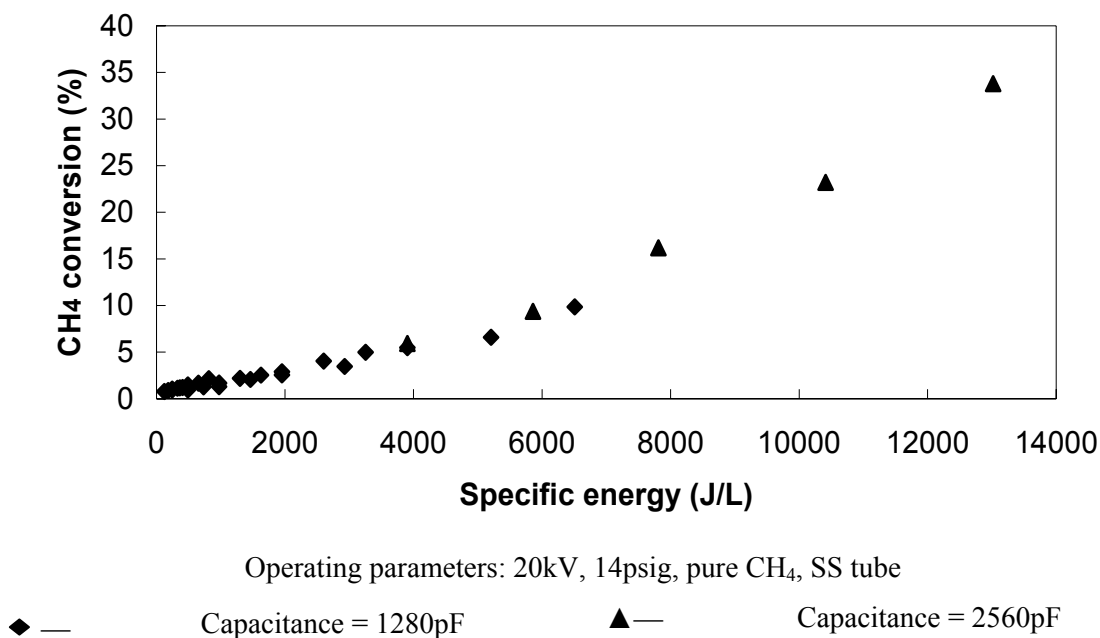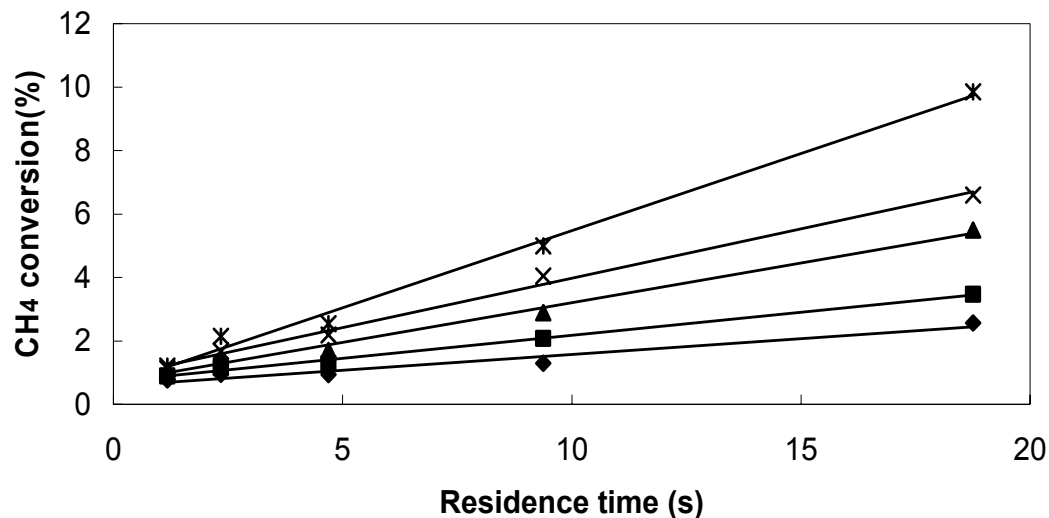

Operating parameters: 20kV, 14psig, pure CH_4, SS tube

◆ —   Capacitance = 1280pF   ▲—   Capacitance = 2560pF

Figure 5. Methane conversion as a function of specific energy input (power per volumetric gas flow rate).

Influence of residence time on methane conversion: Figure 6 shows the influence of residence time on methane conversion with power (or alternatively frequency) as a parameter. The residence time ranged from 18.8 s to 1.18 s, corresponding to flow rates from 39.4×10^{-6} m^3/s to 630×10^{-6} m^3/s (5 to 80 ft^3/h). The data in Figure 6 show that methane conversion increases approximately linearly with residence time at input fixed power. This result suggests that more radicals are being produced at longer residence times relative to shorter residence times.

Operating parameters: 20KV, 1280pF, 14psig, pure CH_4, SS tube

|	Power / Frequency (Watts / Hz)		Power / Frequency (Watts / Hz)
◆—	76.8 / 300	■—	115.2 / 450
▲—	153.6 / 600	×—	204.8 / 800
*—	256 / 1000		

Figure 6. Methane conversion as a function of residence time (flow rate) and power input.

System energy efficiency: The system energy efficiency, as defined by Eq. (8), includes inefficiencies or energy losses in the electrical system as well as the reactor. Calculated system efficiencies approached 40% at low specific energy and low conversion. At high specific energy (greater than 1000 J/l) the system efficiency was relatively constant at approximately 8%. This compares well with the results of other investigators who have calculated First Law thermodynamic efficiency. For example, Zhang et al.[31] and Zhu et al.[30] both report efficiencies of less than 10% for reactors with a much smaller thoughputs of 300 ml/min (0.64 ft^3/h). Table 3 compares the results of this work with those of other investigators of plasma processes for methane conversion.

Table 3. Comparison with other plasma processes

	This work	Fincke[8]	Yao[15]	Yang[5]	Yao[11]	Yao[1]	Yao[18]	Yang[12]	Zhu[13]
Plasma mode	CAC pulsed corona discharge	Continuous plasma	Point to point corona discharge	Corona CAC discharge	Point to point corona discharge	CAC Corona discharge	CAC corona discharge	Glowing discharge	CAC Corona discharge
Feedstock tested	CH_4	CH_4	CH_4	CH_4	CH_4	CH_4	$CH_4:CO_2$ =1:1	CH_4	CH_4
Pressure (psig)	14	0	0	0	0	0	0	0	0
Inlet temperature	Room temp	2000°C	Room temp	Room temp	Room temp	Room temp	Room temp	Room temp	Room temp
CH_4 flow rate ($\times 10^{-6} m^3/s$)	39.4 - 630	1170	5.0	0.333	0.5	2.5	3.33		0.417
CH_4 conversion (%)	3-35	100	40	60	39	40	86		44.6
Energy efficiency (%)	10-45	25	51.38	<10	47	18	15.6	2.34	8
Frequency (Hz)	300-1000	–	9920	1000-2000	8130	9000	10,300	–	66

Influence of electrodes on methane conversion: Figure 7 shows the influence of electrode (cathode) materials on methane conversion. Compared with the stainless steel tube, the niobium membrane and the platinum coated stainless steel tube result in significantly higher conversion. For example, at the highest input power, the conversion is 51% for the niobium and platinum coated stainless steel tubes compared to 33.8% for the stainless steel tube, which is consistent with the results of Spiess et al.[46] In their results, methane conversion is also higher when noble metal electrodes are used. The results in Figure 7 indicate very little difference in conversion between the niobium membrane and the platinum coated tubes. Compared to stainless steel cathodes, this implies that niobium and platinum produce similar catalytic enhancements or that the electrical discharge is more efficient with niobium and platinum cathodes. The hydrogen permeance of the niobium membrane [3.0 x 10^{-10} mol s^{-1} Pa^{-1} m^{-2} (2.0 x 10^{-8} mol s^{-1} atm^{-1} in^{-2})] appears to be too low for superpermeability. Liu et al.[44] postulate that the corona discharge and charged plasma species may lead to charge accumulation on the cathode surface. This could alter the electrostatic potential and/or work function of the metal surface.
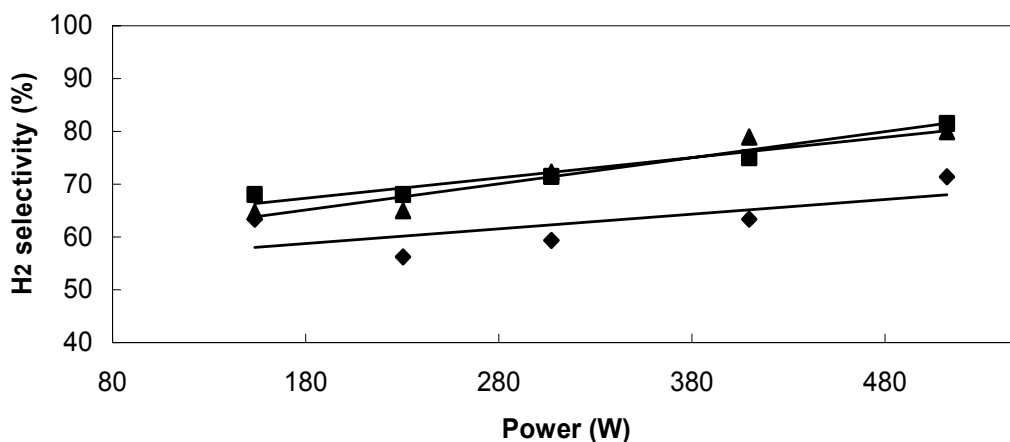
Operating parameters: 20kV, 2560pF, 1000Hz, 14psig, pure CH$_4$

◆ —　　　　　　　SS　　　　　　　■—　　　　　　　Nb

▲—　　　　　　　Pt/SS
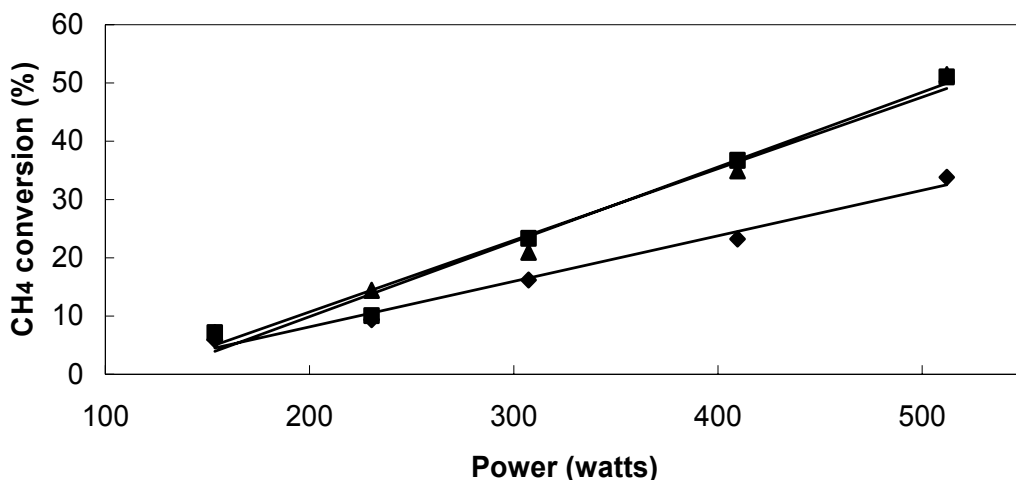
Figure 7. Influence of cathode material on methane conversion.

Selectivity of products: Figure 8 illustrates the influence of input power on H$_2$ selectivity with different electrodes. With the increase of input power, H$_2$ selectivity generally increases for all electrodes. The H$_2$ selectivity ranges from 60 to 70% for stainless steel (SS) and from 65 to 80% for the Pt/SS and Nb tubes. The influence of electrodes on H$_2$ selectivity is similar at all methane conversions.

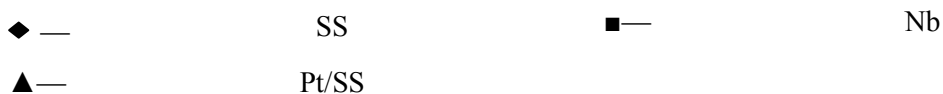Operating parameters: 20kV, 2560pF, 1000Hz, 14psig, pure CH$_4$

◆ —　　　　　　　SS　　　　　　　■—　　　　　　　Nb

▲—　　　　　　　Pt/SS

Figure 8. Influence of input power on H$_2$ selectivity

Figure 9 shows the maximum, average and minimum selectivity for acetylene, ethane and ethylene, propane, and propylene in the products from the stainless steel cathode. Acetylene has the highest selectivity, ranging from 50% to 60%, over the range of experimental parameters studied, which was significantly higher than that for the other products under all operating conditions. The mechanisms for acetylene formation is assumed to be the following based on previous studies:[47, 48]

$$CH_2 + CH_2 \rightarrow C_2H_2 + H_2 \qquad\qquad (R8)$$

$$CH + CH \rightarrow C_2H_2 \qquad\qquad (R9)$$

$$CH_2 + CH \rightarrow C_2H_2 + H \qquad\qquad (R10)$$

$$C_2H_4 \rightarrow C_2H_2 + H_2 \qquad\qquad (R11)$$

Operating parameters: 20kV, 1280pF, 14psig, pure CH_4, SS tube
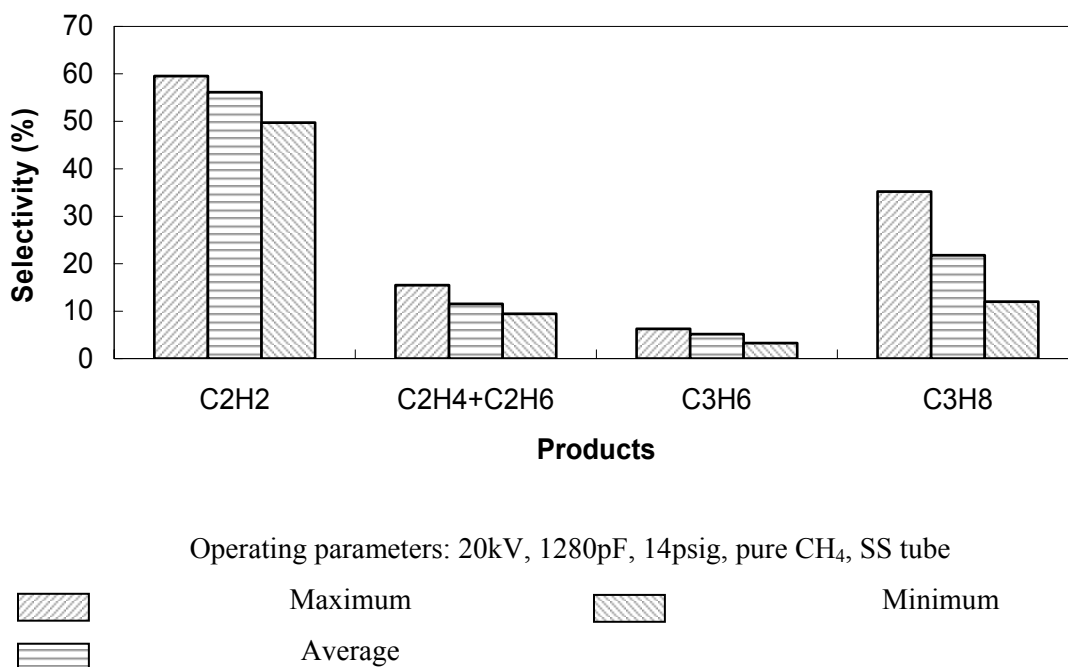
Maximum   Minimum

Average

Figure 9. Range of hydrocarbon selectivities

Due to the small amount of ethane and ethylene in the products and similar characteristic peaks for the two species, the RGA data did not produce accurate or repeatable results for their individual concentrations. Therefore, only the sum of the concentrations of ethane and ethylene in the products is reported. The selectivity for ethane and ethylene combined is approximately

10% at all experimental conditions. The formation of ethane and ethylene is assumed to result from the following reactions:

$$CH_2 + CH_2 \rightarrow C_2H_4 \tag{R12}$$

$$CH_3 + CH_2 \rightarrow C_2H_4 + H \tag{R13}$$

$$CH_3 + CH_3 \rightarrow C_2H_6 \tag{R14}$$

$$CH_4 + CH_2 \rightarrow C_2H_6 \tag{R15}$$

The selectivity for ethane and ethylene is lower, compared with acetylene, indicating CH radicals are the most important species during the methane dissociation process, and (R11) - (R15) do not play a significant role in the process.

Propylene and propane were also measured at significant concentrations (respectively averaging 4% and 20% over the range of experimental parameters studied). This is in contrast to previous results[18, 19, 30] that did not report significant propane production. The following reactions result in the formation of propylene and propane:

$$C_2H_6 + e \rightarrow C_2H_5 + H + e \tag{R16}$$

$$C_2H_5 + CH \rightarrow C_3H_6 \tag{R17}$$

$$C_2H_5 + CH_3 \rightarrow C_3H_8 \tag{R18}$$

As shown in Figure 9, the selectivity for propane is higher than that for the propylene, implying that CH_3 radicals are more plentiful than CH radicals and that (R17) does not contribute significantly to product formation under the experimental conditions of this study.

The sum of the selectivities for acetylene, ethylene, ethane, propylene, and propane is less than 100%, which agrees with the results of Hsieh et al.[27] This discrepancy is the result of carbon lost through the formation of soot and the deposition of carbon or polymer films and other unquantified higher hydrocarbons.[22] A significant amount of carbon formed near the reactor outlet at high pulse frequencies, greater than 600 Hz, and low flow rates, 39.4×10^{-6} and 78.7×10^{-6} m^3/s (5 and 10 ft^3/h), indicating that the CH and CH_2 radicals formed previously were dehydrogenated, as in (R5) and (R6). The molar hydrogen to carbon ratios of 3.98 observed for the two higher flow rates are the same as the feed (which is 4) within the accuracy of the data and provide a check of the mass balance. However, values greater than 3.98 suggest carbon deposition. Based on the ratio of hydrogen/carbon calculated at the outlet (Figure 10), more carbon deposition occurs at low flow rates and higher pulse frequencies (corresponding to higher

power inputs). To avoid carbon deposition, the desired hydrocarbons must be produced in as short a time as possible and quenched. Regarding carbon formation, (R7) is a potential mechanism, but this is inherently a kinetically limited process.[25] The other mechanisms are associated with polymerization and higher hydrocarbon formation.[31] Further investigations are needed to better understand the mechanism of carbon deposition.
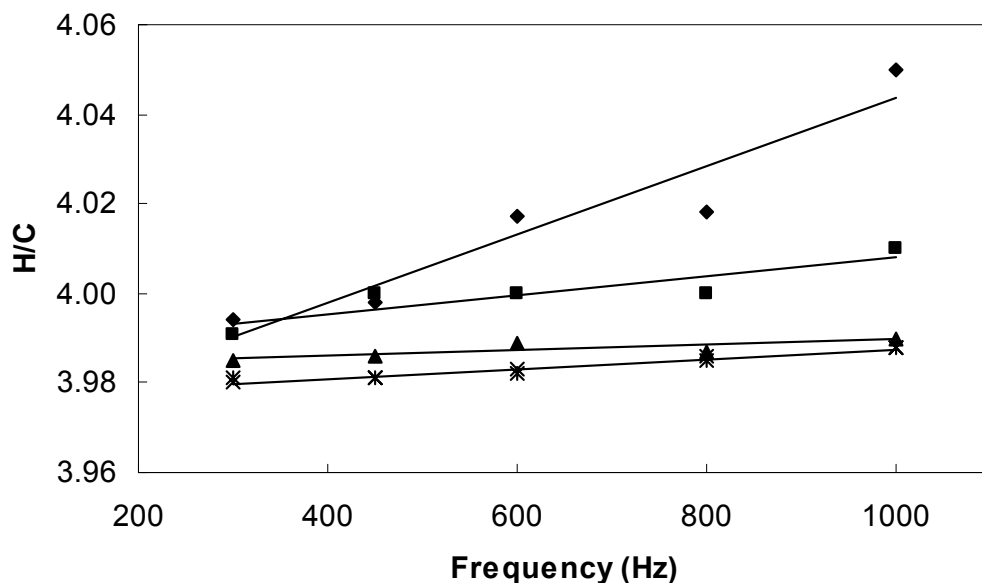
Operating parameters: 20KV, 1280pF, 14psig, pure CH_4, SS tube

	Flowrate ($\times 10^{-6} m^3/s$)		Flowrate ($\times 10^{-6} m^3/s$)
◆—	39.35	■—	78.7
▲—	157.4	×—	314.8
*—	629.6		

Figure 10. Hydrogen to carbon ratio in products (including H_2) as a function of pulse frequency.

Conclusion

This study describes an experimental effort to convert methane to hydrogen and light hydrocarbons using a plasma reactor that can accommodate relatively high flow rates. The reactor is a co-axial cylinder (CAC) pulsed corona discharge reactor driven by a thyratron switch. Methane was introduced to the reactor at room temperature and 198 kPa absolute (14

psig) at flow rates up to 655×10^{-6} m^3/s (80 ft^3/h). The conclusions are listed in the following summary:

- Frequency, capacitance, and charge voltage all have an effect on methane conversion. An increase in any of the three electrical parameters resulted in increased conversion at fixed residence time or flow rate. All contribute to the power input or specific energy, which appears to be the most important factor influencing methane conversion.

- Residence time also had a significant effect on conversion, with longer residence times resulting in higher conversion. This again is a manifestation of the increase in specific energy.

- System energy efficiency was typically in the range of 8%, except under conditions where the conversion was very small (less than 3%) at low specific energy (less than 1000 J/l), when it increased as high as 40%.

- Cathode composition has a large influence on methane conversion and H$_2$ selectivity. At high specific energies, platinum coated stainless steel and niobium membrane cathodes produced methane conversions as high as 51% and H$_2$ selectivities as high as 80%, while the stainless steel cathode produced just under 34% conversion and 60% H$_2$ selectivity.

- Beside hydrogen, acetylene is the primary product, with selectivities ranging from 50 to 60% for the range of parameters studied. Propane selectivity was 10 to 30% while ethane, ethylene and propylene selectivities were always less than 10%.

This study involved the same experimental techniques and equipment that will be used during the initial H$_2$S decomposition experiments. An understanding of the reaction parameter space, which includes pulse frequency, discharge capacitance and voltage, reactor residence time, and electrode material, is vital to optimize reactor performance and energy efficiency. The electrode material effect on the corona discharge and reaction efficiency is particularly important because the multi-layered membranes which will be used as electrodes may alter the corona discharge in ways that were not anticipated when the proposal was written. H$_2$S decomposition will undoubtedly present other challenges that have not been addressed with this methane study, such as handling the liquid and solid sulfur product, but this work has provided significant insight on the important parameters and potential pitfalls that will be faced.

The results of the methane study have already prompted an improvement in the reactor design which has increased its energy efficiency, perhaps by eliminating an electrical arc and permitting more energy to be dissipated in the corona discharge. The data presented in this report were obtained using the older reactor design. The reactor energy efficiency appears to have improved by 30 to 50% compared to the old design, but these results were obtained too recently to include in the body of the report. However, this report will be modified with the recent data and submitted for publication in a peer-reviewed journal.

Further, the single-layer niobium membrane used in this study has provided ideas on improving the efficiency of the multi-layered membranes that are being fabricated for the H_2S experiments. The membrane proximity to the source of the H atoms appears to be very important. Data from N_2 plasmas show that the active species in the plasma are formed near the surface of the anode soon after the discharge pulse,[49,50] which suggests the need to make the membrane the anode in order to achieve effective H atom transport to the membrane surface. This and other improvements will be incorporated in a new reactor and membrane test cell design.

Acknowledgments

References

1. Maddox, R. N. Gas *Conditioning and Processing—Volume 4 Gas and Liquid Sweetening*, Campbell Petroleum Series, Norman, OK, **1982**.

2. West, J. R. Sulfur Recovery, *Kirk-Othmer Encyclopedia of Chemical Technology*, 22 Martin Grayson (Editor), Wiley, New York, **1984**.

3. Strickland, J. F.; Velasquez, D. Topical Report—*Assessment of Recovery Capabilities and Costs of Tail Gas Clean Up Processes*, GRI Contract # 5088-221-1753, **2000**.

4. Zaman, J.; Chakma, A. *Fuel Proc. Tech.* **1995**, *41*, 159.

5. Kaloidas, V.; Papayannakos, N. Kinetics of thermal, non-catalytic decomposition of hydrogen sulfide. *Chem. Eng. Sci.* **1989**, *44*, 2493.

6. Chivers, T.; Lau, C. The thermal decomposition of hydrogen sulfide over vanadium and molybdenum sulfides and mixed sulfide catalysts in quartz and thermal diffusion column reactors. *Int. J. Hydrogen Energy* **1987**, *12*, 235.

7. Fukuda, K.; Dokiya, M.; Kameyama, T.; Kotera, Y. Catalytic Decomposition of Hydrogen Sulfide. *Ind. Eng. Chem. Fund.* **1978**, *17*, 243.

8. Nishizawa, T.; Tanaka, H.; Hirota, K. Decomposition of hydrogen sulfide and enrichment of hydrogen produced by use of thermal diffusion columns? *Intl. Chem. Eng.* **1979**, *19*, 517.

9. Haas, L. A.; Khalafalla, S. E. *Decomposition of Hydrogen Sulfide in an Electrical Discharge*, U.S. Bureau of Mines Report of Investigation 7780, **1973**.

10. Traus, I.; Suhr, H.; Harry, J. E.; Evans, D. R. Application of a rotating high-pressure glow discharge for the dissociation of hydrogen sulfide. *Plasma Chem. Plasma Proc.* **1993**, *13*, 77.

11. Helfritch, D. J. Pulsed corona discharge for hydrogen sulfide decomposition. *IEEE Trans. Ind. Appl.* **1993**, *29*, 882.

12. Harkness, J. B. L.; Gorski, A. J.; Daniels, E. J. Recovery of hydrogen and sulfur from hydrogen sulfide-containing waste gases. U.S. Patent 5211923, **1993**.

13. Bagautdinov, A. Z.; Jivotov, V. K.; Eremenko, J. I.; Kalachev, I. A.; Musinov, S. A.; Potapkin, B. V.; Pampushka, A. M.; Rusanov, V. D.; Strelkova, M. I.; Fridman, A. A.; Zoller, V. A. Hydrogen sulfide dissociation in high pressure microwave discharge with power up to 1 MW. *High Temp. Chem. Proc.* **1993**, *2*, 47.

14. Bagautdinov, A. Z.; Jivotov, V. K.; Eremenko, J. I.; Kalachev, I. A.; Musinov, S. A.; Potapkin, B. V.; Pampushka, A. M.; Rusanov, V. D.; Strelkova, M. I.; Fridman, A. A.; Zoller, V. A. Plasma chemical production of hydrogen from H_2S-containing gases in MCW discharge. *Intl J. Hydrogen Energy* **1995**, *20*, 193.

15. Jivotov, V.; Rusanov, V. Energy cost of plasmachemical hydrogen from hydrogen sulfide is actually not more than about one kWh per cubic meter. *Intl J. Hydrogen Energy* **1999**, *24*, 83.

16. Abolentsev, V. A.; Korobtsev, S. V; Medvedev, D. D.; Rusanov, V. D.; Shiryaevsky, V. L. in *Non-thermal Plasma Techniques for Pollution Control*; Penetrante, B. M.; Schultheis, S. E., Eds.; NATO ASI Series, Vol G 34, Part B; Springer-Verlag, Berlin; **1993**, 139.

17. *CRC Handbook of Chemistry and Physics*, 73rd ed.; Lide, D. R., Ed.; CRC Press: Boca Raton, FL, **1992**.

18. Yao, S. L. Nakayama, A.; Suzuki, E. Methane conversion using a high-frequency pulsed plasma: Important factors. *AIChE Journal*, **2001**, *47*(2), 413-418.

19. Yao, S.L.; Nakayama, A.; Suzuki, E. Methane conversion using a high-frequency pulsed plasma: Discharge features. *AIChE Journal*, **2001**, *47*(2), 419-223.

20. Gladisch, H. How fuels makes acetylene by DC arc. *Hydrocarbon Processing & Petroleum Refiner*. **1962**, *41*(2), 159-164.

21. Holmen, A.; Olsvik, O.; Rokstad, O. A. Pyrolysis of natural gas: Chemistry and process concepts. *Fuel Process. Tech*. **1995**, 249.

22. Yang, Y. Direct non-oxidative methane conversion by non-thermal plasma: experimental study. *Plasma Chemistry and Plasma Processing*. **2003**, *23*(2), 283-296.

23. Bromberg L.; Cohn, D.R.; Rabinovich, A. Plasma reforming of methane. *Energy & Fuels*. **1998**, *12*, 11-18.

24. Bromberg, L.; Cohn, D.R.; Rabinovich, A.; Alexeev, N. Plasma catalytic reforming of methane. *International Journal of Hydrogen Energy*, **1999**, *24*, 1131-1137.

25. Fincke, J. R.; Anderson, R. P.; Hyde, T.; Detering, B.A.; Wright, R.; Bewley, R.L.; Haggard, D.C.; Swank,W. D. Plasma thermal conversion of methane to acetylene. *Plasma Chemistry and Plasma Processing*, **2002**, *22*(1), 105-136.

26. Fincke, J. R.; Anderson, R. P.; Hyde, T. A.; Detering, B. A. Plasma pyrolysis of methane to hydrogen and carbon black. *Ind. Eng. Chem. Res.,* **2002**, *41*, 1425-1435.

27. Hsieh, L.-T.; Lee, W.-J.; Chen, C.-Y.; Chang, M.-B.; Chang, H.-C. Converting methane by using an RF plasma reactor. *Plasma Chemistry and Plasma Processing*. **1998**, *18*(2), 215-239.

28. Yao, S.L.; Nakayama, A.; Suzuki, E. Acetylene and hydrogen from pulsed plasma conversion of methane. *Catalysis Today*, **2001**, *71*, 219-223.

29. Yang, Y. Methane conversion and reforming by nonthermal plasma on pins. *Ind. Eng. Chem. Res.*, **2002**, *41*, 5918-5926.

30. Zhu, A.; Gong, W.; Zhang, X.; Zhang, B. Coupling of methane under pulse corona plasma. *Science in China (Series B),* **2000**, *43*(2), 208-214.

31. Zhang, J.-Q.; Yang, Y.-J.; Zhang, J.-S.; Liu, Q.; Tan, K.-R. Non-oxidative coupling of methane to C_2 hydrocarbons under above-atmospheric pressure using pulsed microwave plasma. *Energy & Fuels*, **2002**, *16*, 687-693.

32. Yao, S.L.; Suzuki, E.; Meng, N.; Nakayama, A. A high-efficiency reactor for the pulsed plasma conversion of methane . *Plasma Chemistry and Plasma Processing*. **2002**, *22*(2), 225-237.

33. Yao, S.L.; Suzuki, E.; Nakayama, A. The pyrolysis property of a pulsed plasma of methane. *Plasma Chemistry and Plasma Processing*. **2001**, *21*(4), 651-663.

34. Yao, S. L.; Suzuki, E.; Meng, N.; Nakayama, A. Influence of rise time of pulse voltage on the pulsed plasma conversion of methane. *Energy & Fuels*, **2001**, *15*, 1300-1303.

35. Yao, S. L.; Okumoto, M.; Nakayama, A.; Suzuki, E. Plasma reforming and coupling of methane with carbon dioxide. *Energy & Fuels*. **2001**, *15*, 1295-1299.

36. Yang, Y. Direct non-oxidative methane conversion by non-thermal plasma: modeling study. *Plasma Chemistry and Plasma Processing*. **2003**, *23*(2), 327-346.

37. Liu, C.-J.; Xue, B.; Eliasson, B.; He, F.; Li, Y.; Xu, G.-H. Methane conversion to higher hydrocarbons in the presence of carbon dioxide using dielectric-barrier discharge plasma. *Plasma Chemistry and Plasma Processing*. **2001**, *21*(3), 301-310.

38. Savinov, S. Y.; Lee, H.; Song, H. K.; Na, B.-K. The effect of vibrational excitation of molecules on plasma chemical reactions involving methane and nitrogen. *Plasma Chemistry and Plasma Processing*. **2003**, *23*(1), 159-173.

39. Zyn, V. I. Kinetic identification of a mechanism of complex plasma chemical reactions. *Plasma Chemistry and Plasma Processing*, **1998**, *18*(3), 395-407.

40. Mutsukura, N.; Handa, Y. Deposition of diamond-like carbon film in a closed-space CH_4 RF plasma. *Plasma Chemistry and Plasma Processing*, **2002**, *22*(4), 607-617.

41. Chen, J.; Davidson, J. H. Ozone production in the positive DC corona discharge: Method and comparison to experiments. *Plasma Chemistry and Plasma Processing*, **2002**, *22*(4), 495-522.

42. QMS 100 Series Gas Analyzer, User's Manual, Stanford Research System, **2000.**

43. Didden, C.; Duisings, J. On-line measurement of a liquid reactor feed with a mass spectrometer. *Process Control and Quality*, **1992**, *3*, 263-271.

44. Liu, C.-J.; Mallinson, R.; Lobban, L. Nonoxidative methane conversion to acetylene over zeolite in a low temperature plasma. *Journal of Catalysis*, **1998**, *179*, 326-334

45. Brown, S. C. Introduction to electrical discharges in gases: *Chapter 11*, DC breakdown. **1966**, John Wiley & Son Inc.

46. Spiess F. J.; Suib, S. L.; Irie, K.; Hayashi, Y.; Matsumoto, H. Metal effect and flow rate effect in the hydrogen production from methane. *Catalysis Today*. **2004**, *89*, 35-45.

47. Hiraoka, K; Aoyama, K.; Morise, K. A study of reaction mechanism of methane in a radio-frequency glow discharge using radical and ion scavengers. *Canadian Journal Chemistry*. **1985**, *63*, 2899-2905.

48. Heintze, M.; Magureanu, M.; Kettlitz, M. Mechanism of C_2 hydrocarbon formation from methane in a pulsed microwave plasma. *Journal of Applied Physics*, **2002**, *92*(12), 7022-7031.

49. Simek, M. Determination of $N_2(A_3\Sigma_u^+)$ metastable density produced by nitrogen streamers at atmospheric pressure. Part 1. Design of diagnostic method. *Plasma Sources Sci. Tech.* **2003**, *12*, 421.

50. Simek, M. Determination of $N_2(A_3\Sigma_u^+)$ metastable density produced by nitrogen streamers at atmospheric pressure. Part 2. Experimental verification. *Plasma Sources Sci. Tech.* **2003**, *12*, 454.

Nomenclature

C	capacitance, F,
f	pulse frequency, Hz
F_0	flowrate at the inlet, m^3/s
F_1	flowrate at the outlet, m^3/s
ΔH_i	reaction enthalpy of the i-th reaction for hydrocarbons, kJ/mol CH_4
$I(m)$	measured current intensity at mass m
$\vec{I}$	vector containing the measured current intensities
m	mass of selected ion
n	carbon number in a molecule
N_0	moles of methane at the inlet, mol
N_1	moles of methane at the outlet, mol
$P(j)$	partial pressure for component j
$\vec{P}$	vector of estimated partial pressure for each component
$S(m, j)$	sensitivity factor of component j at mass m
S	two-dimensional matrix containing the sensitivity factor of the j component at specified mass, m
S^t	transpose of S
S_{Cn}	selectivity of the C_2 and C_3 hydrocarbons, %
T	residence time for pure methane in reactor, s
v	reactor volume, m^3
V	charge voltage, volts
W	the input power, watts
W_p	the specific energy, J/l
X	the CH_4 conversion, %
x_0	mole fraction of methane at the inlet, %
x_1	mole fraction of methane at the outlet, %
Y_{Cn}	yield of C_2 and C_3 hydrocarbons, %
η	energy efficiency based on the First Law, %